Modeling Self-Assembly of Nanoparticles: Cooperative Sequential Adsorption with Evaporation and Time-Varying Rates

A. M. Seredinski

Department of Physics and Engineering, Washington and Lee University, Lexington, VA, 24450

E-mail: seredinskia14@mail.wlu.edu

Abstract.

I review several cooperative sequential adsorption (CSA) approaches with and without evaporation to modeling particle deposition in ionic self-assembled monolayers (ISAM). I then build on the mean field method by introducing time-varying deposition rates that provide greater flexibility in convergence behavior to the steady state of the system. I compare this both with preliminary experimental data, and the mean field method with constant deposition rates.

1. Introduction

The fabrication of nanoscale structures is an area of continuing interest in physics, materials science, and chemistry. One bottom-up method is self-assembly, in which the components are put together and persuaded to arrange themselves into the desired configuration. Thin films have been assembled using layer-by-layer self-assembly, which can be a very reliable and controllable method for coating substrates [1].

This project is motivated by ionic self-assembled monolayers (ISAM), a layer-by-layer technique in which one coats a charged substrate with an oppositely charged material, and can continue to build additional layers by alternating deposited charges. This has been implemented successfully to create antireflective coatings using a glass slide substrate and alternating layers of a polycation "glue" and negatively charged silica nanoparticles [2, 3]. Figure 1 provides a diagram of the process. Coatings of the polymer "glue" (PDDA) and silica nanoparticles are alternated with rinses in deionized water. Under many deposition conditions, the coating will include void space between

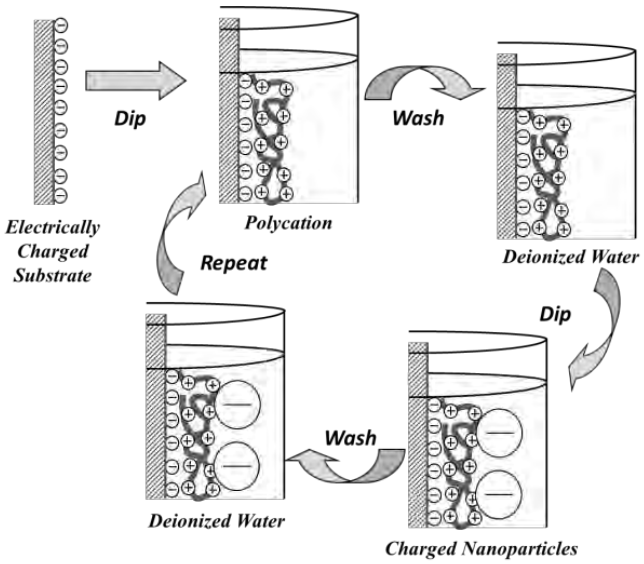

Figure 1. The main steps of the ionic self-assembly of monolayers process

the particles. This is to be expected, as the silica nanoparticles share the same charge and ought to repel one another. This void space is important as it impacts the eventual optical properties of the film, and so modeling and predicting it is of potential value.

The attachment of nanoparticles to the charged polymer is a stochastic process. Two basic approaches have been used with relative success to model the depositions: random sequential adsorption (RSA) [4, 5, 6] and cooperative sequential adsorption (CSA) [7]. In RSA models, particle attachment is modeled by the random deposition of particles at a fixed rate onto a lattice or graph. RSA models are so general as to work for a lattice of any dimension or indeed a graph of any geometry, as the interconnection of lattice sites is unimportant for a random process. CSA models differ in that the

likelihood of particle deposition depends on the presence (and number) of neighboring, occupied sites.

CSA models in two-dimensions (and higher) are not as well understood as those in the easily solvable one-dimensional case. They are, however, exactly solvable on a Cayley tree - a finite, cycle-free graph with each node connected to z other neighbors, where z is known as the coordination number. A Cayley tree of coordination number

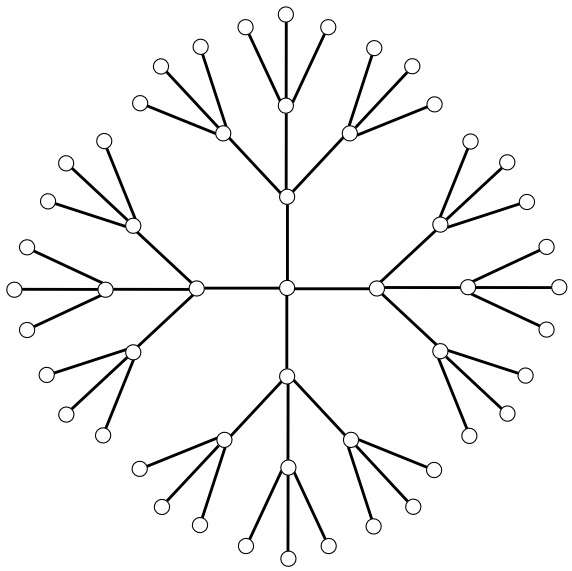

Figure 2. Cayley tree with coordination number z=4

$z = 4$ has been used to approximate a two-dimensional lattice with a high degree of success [4]. Analytic results on Cayley trees and their infinite analogue the Bethe lattice have more recently been published [8, 9, 10, 1].The Cayley tree is of particular interest in ISAM due to a type of polymer known as a dendrimer which has the same structure as a Cayley tree and can be used as the polymer "glue" in layer-by-layer self-assembly. Dendrimers have high potential for use as a novel drug delivery mechanism through drug encapsulation and so are an area of interest in nanotechnology and nanomedicine [11, 12].

I am particularly interested in advancing understanding of cooperative sequential adsorption with evaporation (CSAE) models. The model proposed in this thesis is more general than most CSA models, as it allows for particles to both attach *and* detach from the surface with different, time-varying deposition rates. While standard CSA models account for much of the time-dependent deposition behavior in ISAM, including a time-dependent deposition rate could allow for curves that better agree with current data qualitatively. The data appears to break into two main time regimes - one of very high adsorption followed by one of adsorption at a more modest rate [13]. This could be precisely accounted for by the insertion of time-varying deposition rates into a CSAE model.

Such a model would also have potential applications outside of ISAM. Epidemic-

type models, including voter models, rumor-spreading models, and computer virus models, are well-represented in the literature, and some applications could easily be made to fit with a Cayley tree based CSAE model [14, 15, 16]. In fact, the model that I propose can be applied beyond a Cayley tree to any graph in which each site is connected to a specific number of other sites. This includes square lattices.

This thesis will begin with an overview of the work done so far on CSA models on Cayley trees with special attention given to the work of *Mazilu et al.* [1, 17] and *Cook et al.* [18] which serves as the direct background to this work. This overview will begin in section 2 with an explanation of the empty interval method and its results on Cayley trees. It will then document mean field approaches beginning with an analogy of particle deposition to the Ising model (section 3) and concluding with a more general approach (section 4). This will serve as the direct foundation for the novel model described in section 5 which employs time-varying rates. The numerical results of this method will be compared with experimental particle deposition data from ISAM and with the results of the standard mean field method in section 6. Finally, section 7 will serve to summarize the conclusions of this project and outline future directions.

2. The Empty Interval Method

The primary interest with a CSA model is to determine adsorption behavior at sites while taking into account adsorbate-adsorbate interactions. Consider the following set of depositions on a Cayley tree, where "$\circ$" represents an unfilled or open node and "$\bullet$" represents a filled node [8]:

$\bullet\circ \rightarrow \bullet\bullet$ with rate r_1.
$\circ\circ \rightarrow \bullet\circ$ with rate r_2.
$\circ\circ \rightarrow \bullet\bullet$ with rate r_3.

Left and right are arbitrary in this visualization ($\bullet\circ$ is not a state distinct from $\circ\bullet$). There is then no diffusion of particles throughout the substrate post-adsorption. Note that these rates allow for both monomer and dimer deposition. Dimers are included in this model because SEM images of self-assembled coatings of silica present with dimers.

The empty interval method itself "tracks" clusters of empty nodes on the graph. We define E_n as the probability of n connected nodes on the Cayley tree all being empty, regardless of the occupation of the other nodes on the tree. Figure 3 shows an example of an E_4 state on a tree with $z = 3$. Importantly, E_1 is then the probability of a given node being unoccupied, meaning that $1 - E_1 = \rho$, where ρ is the particle density on the adsorption surface. The outermost nodes of the tree are treated differently since they are each only connected to one adjacent site. For simplicity, they are here left empty and excluded from calculations of ρ.

Let $P(\bigcirc_n) = E_n$. Consider an additional node connected to this empty n-cluster. That node is either filled or empty. Let $P(\bullet - \bigcirc)$ denote the probability that this

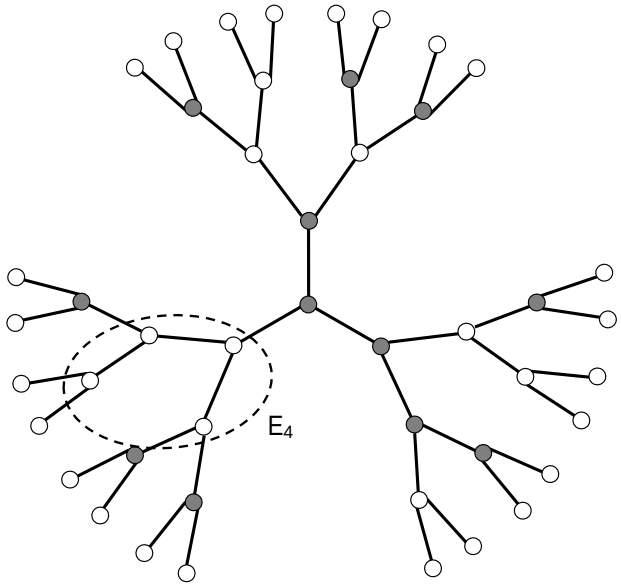

Figure 3. An E_4 state in a partially filled Cayley tree with $z = 3$

n-cluster is connected to a filled node, and $P(\circ - \bigcirc)$ the probability that this n-cluster is connected to an empty node. We have:

$P(\bullet - \bigcirc) + P(\circ - \bigcirc) = E_n$, which in turn means that:
$P(\bullet - \bigcirc) = E_n - E_{n-1}$

Defining these probabilities allows us to construct the evolution equation for the n-cluster. We can find E_n by solving the differential equation that details the ways in which E_n can change. This equation is:

$$\frac{dE_n}{dt} = -(n(z-2)+2)(r_1 P(\bullet - \bigcirc_n) + (r_2 + r_3)E_{n+1}) - (2r_2 + r_3)(n-1)E_n \quad (2.1)$$

It is useful to recognize in this equation that $n(z-2)+2$ is the total number of adjacent nodes to the n-cluster. The first term sums the possibilities of leaving the E_n state considering the states of the nodes just outside of the cluster. The second term sums the possibilities of the n-cluster breaking along any of the $n-1$ connections within the cluster (two possibilities of either node filling with a monomer, and one possibility of both connected nodes filling with a dimer). This equation can be simplified using the relations of the probabilities expressed earlier:

$$\frac{dE_n}{dt} = -\{r_1[n(z-2)+2] + (2r_2+r_3)(n-2)\}E_n - (r_2+r_3-r_1)[n(z-2)+2]E_{n+1} \quad (2.2)$$

Note that the second term disappears in the special case $r_1 = r_2 + r_3$. This yields the relatively simple solution:

$$E_n(t) = e^{-\{n[r_1(z-2)+2r_2+r_3]+2r_1-2r_2-r_3\}t} \tag{2.3}$$

More generally, we assume a solution of the following exponential form:

$$E_n(t) = E_1(t)(\phi(t))^{n-1} \tag{2.4}$$

This yields a system of coupled differential equations (with the terms β and α used for convenience and defined below the system):

$$\frac{d\phi(t)}{dt} = -\beta\phi(t) - \beta\alpha\phi(t)^2 \tag{2.5}$$

$$\frac{dE_1(t)}{dt} = -(zr_1 + \frac{z}{z-2}\alpha\beta\phi(t))E_1(t) \tag{2.6}$$

with

$$\beta = (z-2)r_2 + 2r_2 + r_3 \tag{2.7}$$

$$\alpha = \frac{(z-2)(r_2+r_3-r_1)}{(z-2)r_1 + 2r_2 + r_3} \tag{2.8}$$

Given appropriate initial conditions, we can now solve for the probabilities of interest, beginning with the base case of E_1. Suppose that we begin with an empty Cayley tree, meaning $E_n(t=0) = 1$. This is the case of physical interest to us given the experimental motivation, where the substrate is initially free of nanoparticles. Then we have:

$$E_1(t) = e^{-zr_1t}(\frac{1}{1+\alpha(1-e^{-\beta t})})^{\frac{z}{z-2}} \tag{2.9}$$

$$E_n(t) = e^{-zr_1t-(n-1)\beta t}(\frac{1}{1+\alpha(1-e^{-\beta t})})^{\frac{z}{z-2}+n-1} \tag{2.10}$$

From this, we can calculate the term of experimental interest, $\rho = 1 - E_1$, which is the particle density. Note that with this model, if all rates are nonzero, the final state of the Cayley tree will be entirely full. Setting $r_1 = 0$ models complete electrostatic screening, in which no nanoparticle may adsorb at a node adjacent to an already present nanoparticle. This will eventually result in a "jammed state." Setting $r_3 = 0$ excludes dimers.

A similar method can also be used to create a model for deposition on individual shells of the Cayley tree ("generations" of a dendrimer). Such a model allows one to calculate the probability of specific configurations of particles arising. This technique can also be solved with attachment rates that vary by shell. This would allow for attachment towards the center of the Cayley tree be much more likely. Shell dependent models, including an overall probability for different occupation shells on all states (still requiring empty shells in between), were developed by *Mazilu et al.*[1].

Such an approach could more appropriately model realizable physical scenarios involving dendrimers, which have spaces inside of their tree structure. These spaces are much larger towards the center of the dendrimer. As such, the probability of a dendrimer being able to hold a drug molecule is more likely at nodes towards the center. The models developed by *Mazilu et al.* treat the final shell differently, as a dendrimer can also have molecules attached to its surface [1]. Here there is no internal space limitation. In fact, a dendrimer could carry one sort of molecule inside of its structure and a different one on its outside (e.g. a targeting molecule for drug delivery applications). A shell-dependent model could also more appropriately model a situation in which distance from a certain node (the center) is meaningful. An example of this would be an epidemic model where nodal proximity to the center is a way of representing distance from, for example, a delegate's home constituency in a state-wide election.

3. The Ising Model Analogy Method

One important drawback of the empty interval method is that if evaporation rates are introduced the evolution equation becomes unsolvable. Consider then the Ising model, a two-state system introduced to model spin behaviors and resulting magnetic states which has been solved on a Cayley tree. The Ising Model is interested in the influence of neighboring spins on a given particle's spin and also the impact of an external magnetic field. For a system of N spins interacting with their nearest-neighbors, the well-known Hamiltonian is expressed:

$$H = -J \sum_{i,j \in NN} s_i s_j - B \sum_{i=1}^{N} s_i \tag{3.1}$$

Where each s represents a particle spin of value 1 for spin-up and -1 for spin-down, J is the coupling constant showing the influence of the nearest neighbors on the ith spin (abbreviated NN), and B is the external field.

The Ising model is of particular interest because of its known results [19], two-state nature, and consideration of neighboring states. We wish to construct a CSAE model, and so a model that accounts for flipping between two states based on neighoring occupation is desireable. We define occupation states on a Cayley tree $n_i = 0$ for an empty site and $n_i = 1$ for a filled site. The transition rate may then be expressed:

$$c(n_i \to (1 - n_i)) = \gamma n_i + (1 - n_i)\alpha\beta^{\sum_{j \in NN} n_j} \tag{3.2}$$

The first term is the evaporation term with likelihood γ. Note that if the site is empty, $n_i = 0$, and this transition cannot occur. Similarly, the second term is the deposition term, with background rate α and an influence by nearest neighbor occupation shown by $\beta^{\sum_{j \in NN} n_j}$. This means that if $n_j = 0$ for all adjacent sites (all are empty) there will be no influence by the neighboring sites. We want to account for

electrostatic screening in our model, and setting $0 < \beta < 1$ accounts for the sort of screening we would expect - more occupied neighbors making deposition less likely.

The occupation number of the site can be easily translated into a spin. The new flip-rate is then easily re-expressed in terms of spins.

$$n_i = \frac{1+s_i}{2} \tag{3.3}$$

$$c = \gamma(\frac{1+s_i}{2}) + (\frac{1-s_i}{2})\alpha\beta^{\sum_{j\in NN}\frac{1+s_j}{2}} \tag{3.4}$$

We are primarily interested in the particle density ρ. In terms of occupation number, this is expressed simple as $< n_i >$, or the average occupation state of any site. In terms of spins, we define $q_i =< s_i >$, and the particle density becomes $\rho = \frac{1+q_i}{2}$.

This particle deposition model can now be mapped onto the Ising model. I follow *Mazilu et al.* and include the details of this calculation in Appendix A [17]. The important relations (and notations) are for the coupling constants, K and h:

$$K = \frac{J}{kT} = \frac{1}{4}ln(\beta) \tag{3.5}$$

$$h = \frac{B}{kT} = \frac{1}{4}ln(\frac{\alpha^2\beta^z}{\gamma^2}) \tag{3.6}$$

and the particle density, ρ:

$$\rho = \frac{1+M}{2} \tag{3.7}$$

In these relations, k is the Boltzmann constant, T is the temperature in Kelvin, and M is the magnetization (which can be calculated from the Ising model) and is the same as the mean spin state q_i.

The evolution equation for the magnetization and q_i is then written:

$$\frac{dq_i}{dt} = -q_i(t) + h + < \tanh(K\sum_{j\in NN} s_j) > + h < s_i \tanh(K\sum_{j\in NN} s_j) > \tag{3.8}$$

The evolution of the model now becomes highly dependent upon the Cayley tree in question, as the presence of additional neighboring particles makes the calculations more complicated. Note the dependence of the evolution equation on summations over nearest neighbors, the number of which will vary directly with the coordination number of the Cayley tree. The solution for a Cayley tree with coordination number $z = 3$ will be different than for a Cayley tree with coordination number $z = 4$. I here walk through the solution for $z = 3$. I begin with the case of no external field and then contrast it with the more difficult case of a nonzero external field.

3.1. Zero External Field

Suppose that $h = 0$. Then based on the relationship established in equation 3.6, this means $\frac{\alpha^2\beta^3}{\gamma^2}$ approaches one. This applies to a small subset of situations of interest. Of the three rates, β is the only one with any sway over the coupling constant (which makes

intutitive sense, as β represents the cooperative effect on the deposition). Consider then $\frac{\alpha}{\gamma}$ to be the other quantity of interest. This quotient supplies all of the important steady-state information for the system when combined with β. Then for $h = 0$, we have $(\frac{\alpha}{\gamma})^2 = \beta^{-3}$. This is a very stringent criterion and dramatically decreases the freedom that we have to define rates. For each $\frac{\alpha}{\gamma}$, there is a unique β that will work. Furthermore, since $0 < \beta < 1$, we are implicitly requiring $\alpha > \gamma$. Other limitations include that none of the rates can be zero. For $\beta = 0$, we have constant K and h, meaning a system that does not depend on the other deposition rates at all. Note also that this would not be a case of zero external field. γ is in the denominator and so we have already assumed it to be nonzero. We are not interested when it comes to ISAM in situations that disallow deposition but allow evaporation (perhaps the system starts somewhat full), so $\alpha = 0$ is also not a valid option. Despite the limitations of the zero field case, it is worth exploring as a starting point based on the Ising analogy (where zero external field is of particular interest), and as the model is more widely applicable than particle deposition, and so these conditions may be more meaningful in another context.

In the zero field condition, the evolution equation simplifies significantly to:

$$\frac{dq_i}{dt} = -q_i(t) + < \tanh(K \sum_{j \in NN} s_j) > \tag{3.9}$$

Finding $< \tanh(K \sum_{j \in NN} s_j) >$ is then the challenge. Following *Melin et al.* [20], we use the following relationship:

$$\tanh(K(\sum_{j \in NN} s_j)) = \tanh(K(s_1 + s_2 + s_3)) = C_1(s_1 + s_2 + s_3) = C_2(s_1 + s_2 + s_3)^3 \tag{3.10}$$

where the coefficients C_1 and C_2 are:

$$C_1 = \frac{1}{24}(27\tanh(K) - \tanh(3K)) \tag{3.11}$$

$$C_2 = \frac{1}{24}(\tanh(K) - 3\tanh(3K)) \tag{3.12}$$

The evolution equation can then be written as below. Note that this is only valid for interior nodes on the tree - exterior nodes in the final generation of the Cayley tree are only connected to a single other node, and so are vastly simpler to analyze.

$$\frac{dq_i}{dt} = -q_i(t) + (C_1 + 7C_2) \sum_{j \in NN} q_j + 6C_2 < \prod_{j \in NN} s_j > \tag{3.13}$$

We now make the factorization approximation, decoupling the third order correlations above:

$$< \prod_{j \in NN} s_j > = \prod_{j \in NN} q_j \tag{3.14}$$

Finally, we make the assumption that $q_i(0) = q_j(0)$ if i and j belong to the same generation of the Cayley tree. This is a reasonable assumption for our purposes, as even in the initial configuration is non-empty, we would assume that it would be random on any given generation (note that the cooperative effects have an impact between adjacent generations, as no two nodes on a given generation are connected on the Cayley tree). This means that for any later time t, $q_i(t) = q_j(t)$. This allows us to write (for example) $\sum_{j \in NN} q_j = 3q_j$.

We label the central node of the tree as q_1, and then each subsequent generation from 2 to n is labeled accordingly, with generation n being the outermost generation of the tree, and being governed by a simpler and self-evident equation. This labeling convention differs from that in Melin. The system of equations is:

$$\begin{aligned}
\frac{dq_1}{dt} &= -q_1 + 3(C_1 + 7C_2)q_2 + 6C_2 q_2^3 \\
\frac{dq_i}{dt} &= -q_i + (C_1 + 7C_2)(q_{i-1} + 2q_{i+1}) + 6C_2 q_{i-1} q_{i+1}^2 \\
\frac{dq_n}{dt} &= -q_n + q_{n-1}\tanh(K)
\end{aligned} \tag{3.15}$$

with the index i ranging from 2 to $n-1$.

The nonlinear terms in this system of equations make matrix methods unhelpful for an exact solution, but the system can be readily used for Monte Carlo simulations. One need only choose deposition and evaporation rates.

3.2. Nonzero External Field

We now suppose that there is an external field present, and so $h \neq 0$. This situation is much more widely applicable as it allows for virtually any choice of deposition rates (though the evaporation rate must be nonzero). We use the same expression for $< \tanh(K \sum_{j \in NN} s_j) >$ as in the $h = 0$ case, but must now also solve for $< s_i \tanh(K \sum_{j \in NN} s_j) >$.

$$< s_i \tanh(K(s_1 + s_2 + s_3)) > = C_1 + 7C_2 < s_i s_1 + s_i s_2 + s_i s_3 > + 6C_2 < s_i s_1 s_2 s_3 > \tag{3.16}$$

Once again employing the factorization approximation, assuming that the mean occupancy for sites in the same generation are equal, the same generation-numbering scheme, and using direct substitution, we have the following system of equations:

$$\begin{aligned}
\frac{dq_1}{dt} &= -q_1 + 3(C_1 + 7C_2)q_2 + 6C_2 q_2^3 + h(1 + 3(C_1 + 7C_2)q_1 q_2 + 6C_2 q_1 q_2^3) \\
\frac{dq_i}{dt} &= -q_i + (C_1 + 7C_2)(q_{i-1} + 2q_{i+1}) + 6C_2 q_{i-1} q_{i+1}^2 \\
&\quad + h(1 + (C_1 + 7C_2)(q_i q_{i-1} + 2q_i q_{i+1}) + 6C_2 q_i q_{i-1} q_{i+1}^2) \\
\frac{dq_n}{dt} &= -q_n + q_{n-1}\tanh(K) + h(1 + \tanh(K) q_n q_{n-1})
\end{aligned} \tag{3.17}$$

As with the case of no external field, this system of equations is not exactly solvable via matrix methods due to the nonlinear terms.

4. The Mean Field Method

The Ising model analogy is helpful in that it relates the model in question to one with established applications and results. As seen above, the analogy is drawn by relating the deposition rates to the quantities in the Ising model Hamiltonian through the detailed balance condition. However, an evolution equation can also be determined using our deposition rates without an analogy to the Ising model. This method depends on the mean field approximation, which is essentially just a specific case of the general factorization approximation used in section 3. We follow *Cook et al.* [18]. In taking the average particle density, we approximate:

$$< n_i n_j >=< n_i >< n_i > \tag{4.1}$$

Additionally, we take our particle deposition rate and cast it as its own evolution equation:

$$\frac{dn_i}{dt} = -\gamma n_i + (1 - n_i)\alpha\beta^{\sum_{j\in NN} n_j} \tag{4.2}$$

Using this evolution equation and our mean field approximation, we then have:

$$\frac{d < n_i >}{dt} = -\gamma < n_i > +(1- < n_i >)\alpha\beta^{\sum_{j\in NN} <n_j>} \tag{4.3}$$

Furthermore, assuming that the particles distribute uniformly onto the surface and that they are (by and large) not in boundary sites on the Cayley tree, we eliminate the indexing of each individual site and treat them all similarly:

$$< n_i >=< n > \tag{4.4}$$

Note that in making this assumption, we are actually creating a deposition model that is applicable beyond Cayley trees and to any sort of lattice with a constant connectedness between sites (e.g. a two-dimensional square lattice). In eliminating the differential treatment of different generations of the Cayley tree, and in eliminating the special case of the boundary sites, we have both simplified and generalized the model to a reasonable approximation.

Another important consequence of this approximation is that without indexing, the nearest neighbor summation simplifies: $\sum_{j\in NN} < n >= z < n >$. Returning to the ρ notation for the particle density, we write our evolution equation as:

$$\frac{d\rho}{dt} = -\gamma\rho + (1 - \rho)\alpha\beta^{z\rho} \tag{4.5}$$

The steady state (final fill state) can be determined by setting $\frac{dp}{dt} = 0$. The result is a transcendental equation that can only be solved numerically:

$$\rho_f = \frac{\alpha\beta^{z\rho}}{\gamma + \alpha\beta^{z\rho}} \tag{4.6}$$

5. Generalized Model Definition

There is evidence of nonlinear time dependence in the case of ionic self-assembly of charged silica nanoparticles onto a substrate [13]. This experiment used a silver electrode rather than a charged polymer substrate as in ISAM, though there is no reason to suspect that the adsorption behavior would qualitatively differ given a chemically dissimilar but comparably charged surface. During the first ten seconds of the deposition, a fast Langmuir-type adsorption pattern is followed. After that, with roughly 90% of the deposition completed, there is a slow RSA-type deposition toward the steady-state. While this two-phase model fits the data well, it does not take into account adsorbate-adsorbate interactions (in particular, electrostatic screening), which are known to take place. This is the advantage qualitatively of a CSA model, particularly a more general one that includes the possibility of evaporation. While the CSA models described above do adequately fit the fact that early-time deposition is much more productive than late-time deposition (due to the adsorbate-adsorbate interactions), introducing time-dependent deposition and evaporation rates could further match this behavior.

This will also increase the generality of the model. However, as with the two-stage description in the literature [13], there is a likely departure from the physical situation at play. That is, one would expect the adsorbate-adsorbate interactions themselves to be time-independent and their influence on the deposition to be based solely on the particle density (accounted for by nearest neighbor effects in any CSA model). However, CSAE models would have wider applicability, as discussed in section 1. For example, one might expect in a voter model for proximity to an election date to impact the likelihood of a voter switching their candidate choice, and so a time-varying "flip" rate would be contextually meaningful.

5.1. A Special Case

In a relatively trivial case of time dependent deposition and evaporation rates, we have actually already presented a solution. Suppose $\beta(t) = \beta$ is constant and that $\alpha(t)$ and $\gamma(t)$ are multiples of one another. The Ising analogy in section 3 translates these rates into a spin-spin interaction term (related to K) and an external field term (related to h). K depends only on β. As seen in equation 3.6, h is related to $\frac{\alpha(t)}{\gamma(t)}$. Then so long as $\frac{\alpha(t)}{\gamma(t)} = C$ for some constant C, then we have the solution already from the constant rates case.

Significantly, this shows that the important factor is neither the deposition nor evaporation rate in isolation, but rather their quotient. This being the case, we can define $\alpha(t)$ to be a function and hold γ constant and allow $\alpha(t)$ to behave as what would otherwise be the quotient of the two terms.

5.2. The Model

To qualitatively match the ISAM results, assuming that we are keeping the evaporation rate constant, we need a deposition rate that begins high and then decreases. It is also worth noting that we require a deposition rate that will eventually induce a steady state. Intuitively, we then want a deposition rate that approaches a horizontal asymptote. Consider then the evolution equation from the mean field method, but with the inclusion of time-dependent rates:

$$\frac{d\rho}{dt} = -\gamma\rho + (1-\rho)\alpha(t)\beta(t)^{z\rho} \tag{5.1}$$

If we are interested in a more quickly converging model, we can then have an $\alpha(t)$ that decreases with time down to a certain limit, a $\beta(t)$ that decreases with time down to a certain limit, or a combination of both. Let these limits be α_f and β_f respectively. We have the following steady state equation:

$$\rho_f = \frac{\alpha_f \beta_f^{z\rho}}{\gamma + \alpha_f \beta_f^{z\rho}} \tag{5.2}$$

In the context of ISAM, a decreasing $\beta(t)$ would indicate an increase in the contribution of the adsorbate-adsorbate interactions (or at least a contribution related to the surface coverage - it could be related to the underlying polymer rather than the previously adsorbed particles). This seems to be more or less accounted for by the exponent of the $\beta(t)$ term, especially when the exponent of $\beta(t)$ is written in terms of the overall particle density rather than the "local particle density" (nearest neighbor occupation state). This being the case, we choose to vary $\alpha(t)$ and keep β constant.

A myriad of functions match the desired behavior for $\alpha(t)$. One particularly intuitive option which is easy to manipulate is an exponential. In this case, we have $\alpha(t) = \alpha_0 e^{-\alpha_1 t} + \alpha_2$. Note that $\alpha_2 = \alpha_f$ in equation 5.4. We also are able to intuitively decide upon the initial value of the deposition rate in this way, as $\alpha(0) = \alpha_0 + \alpha_2$. Then α_1 here then serves to set how "quickly" the function converges to α_f. It would seem like we would be able to eliminate α_1 altogether since the time scale of the model is arbitrary. However, this would preclude our comparing different starting α values properly, as without α_1, a higher starting rate would always mean a longer time to an $\alpha(t)$ within some value of α_f. It is worth writing α_0 in terms of α_2 and introducing a scaling factor s, as this will make it easier to understand the relationship $\alpha(0) = (1+s)\alpha_f$.

Finally, then, we are interested in the following evolution equation and accompanying steady state equation:

$$\frac{d\rho}{dt} = -\gamma\rho + (1-\rho)(se^{-\alpha_1 t} + 1)\alpha_f \beta^{z\rho} \tag{5.3}$$

$$\rho_f = \frac{\alpha_f \beta^{z\rho}}{\gamma + \alpha_f \beta^{z\rho}} \tag{5.4}$$

5.3. The Model without Evaporation

Setting $\gamma = 0$, we can examine the time-dependent behavior of such a deposition if no detachment is expected. The steady state becomes uninteresting, as without any evaporation (and $\beta \neq 0$), we have $\rho_f = 1$. The resulting evolution equation is:

$$\frac{d\rho}{dt} = (1-\rho)(se^{-\alpha_1 t} + 1)\alpha_f \beta^{z\rho} \tag{5.5}$$

If we were to introduce $\beta(t)$ such that this function reached zero at some time, perhaps through a piecewise definition, then the model without evaporation would not necessarily result in $\rho_f = 1$, but could also reach some jammed state.

6. Comparisons

6.1. Comparison with Results from ISAM

Mazilu et. al used ISAM to create single bilayers of PDDA "glue" and silica nanoparticles. I analyzed the SEM micrographs to determine their particle coverage. The grayscale values of the micrographs have a bimodal distribution, with particles in general being lighter shades because they stick up from the adsorption surface. Using ImageJ, I made the images dichromatic by picking a grayscale value cutoff between the two modes of the distribution, and eliminating resulting noise. Pixel counts were then employed to determine the slide coverage. Figure 4 shows how the raw SEM and the processed SEM appear. In the black and white processed version, white pixels represent areas occupied by particles.

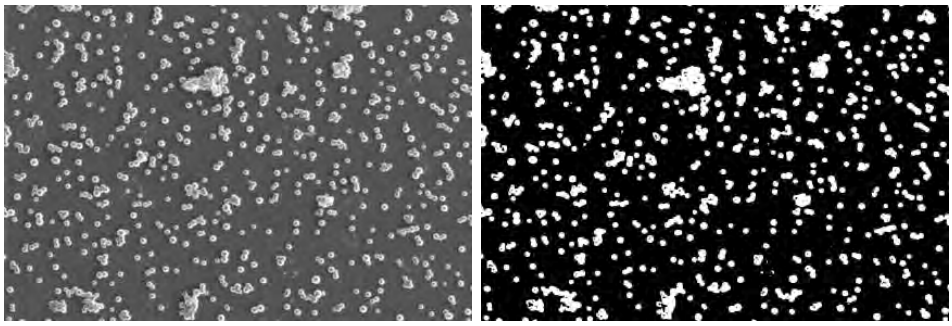

Figure 4. SEM images of ISAM before and after processing with ImageJ

Preliminary time-dependence data was largely inconclusive. However, it appears that the steady state is at least approximately reached within the first two to three seconds of the deposition. This suggests that the initial period of faster deposition is even shorter than the ten second window previously mentioned [13]. Data taken at 1, 2, 3, 5, 10, and 20 seconds is shown in Figure 5. I suggest that this is preliminary data because each dipping time was used on only one slide, and then different sections of the slide were analyzed under the SEM. It seems particularly counterintuitive that the

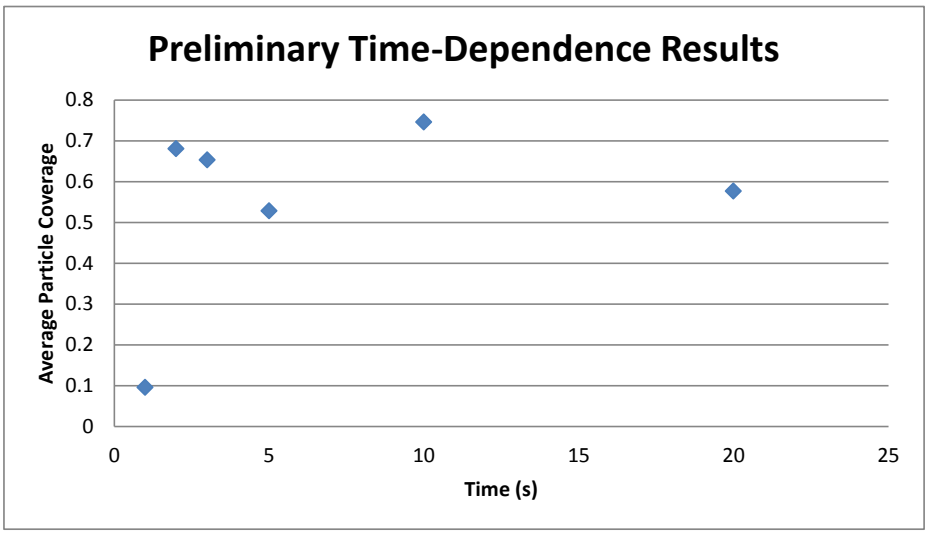

Figure 5. Preliminary ISAM time-dependence data

coverage would vary significantly later in the deposition as is seen in this data, so I interpret this behavior as the presence of a rather large standard deviation in our final coverage resulting from our experimental method. That is, there appears to be no likely mechanism that would take a coverage of (all numbers are used for illustrative purposes) 0.7, and after five seconds lower it to 0.55, and then ten seconds later raise it back up to 0.65. More likely, there is just a great deal of variation in the dipping results. This can already be seen from the standard deviations within individual depositions, and it would seem that even more variability could be expected between them. The standard deviation for the data points taken from the 20 second deposition is greater than 0.075.

The data *does* seem to suggest a steady state reached within three seconds, though the suggestions above regarding a high standard deviation do throw doubt on this hypothesis. Either way, these results are not conclusive enough to show a detailed time-dependent doverage pattern, especially in the region before the steady-state is reached. As such, the advantage of a mean field approach with a time-varying deposition rate over the standard mean field approach remains unclear in experimental application to ISAM. Either method is capable of matching such a vague pattern.

6.2. Comparison with the Mean Field Method

The subtleties added by a time-varying deposition rate are still worth exploring, both in anticipation of more conclusive ISAM data, and towards other applications.

In Figure 6, the particle coverage predicted by the model above is compared against the mean field prediction which uses constant rates. Here, α_1 is varied, which changes the time scale for the convergence of the time-varying deposition rate to reach α_f. Note that the time scale is omitted on the graph because its units are arbitrary. There are two sets of plots, each with two instances of time varying deposition rates ($\alpha_1 = 2$,

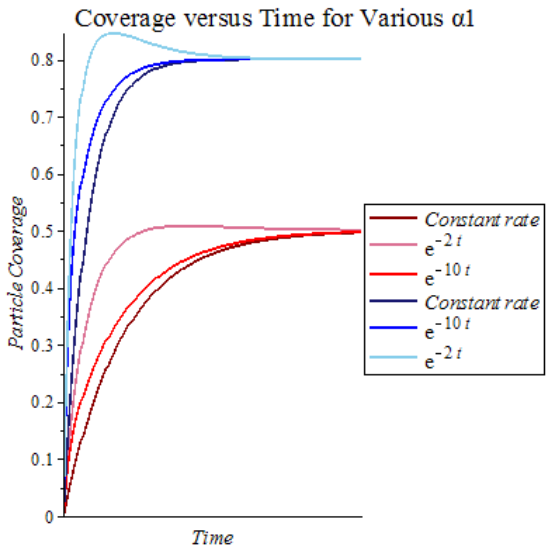

Figure 6. Particle density as a function of time for various α_1 and the mean field solution; $\gamma = 0.5$, $\beta = 1$, $z = 4$, $s = 2$ ($\alpha(0) = \alpha_f$)

10) and the corresponding constant rate mean field solution. The blue / top data has $\alpha_f = 2$ and so a steady-state of 0.8, while the red / bottom data has $\alpha_f = 0.5$ and thus a steady state of 0.5. The lower the α_1 value, the more slowly the deposition rate will approach α_f. The lightest plots for both sets overshoot the steady state because the deposition rate remains high for longer. However, as α_1 increases, this behavior disappears and becomes what is seen in the $\alpha_1 = 10$ plots. The convergence is simply faster. As α_1 continues to increase to arbitrarily large values, the plot converges to the mean field solution, as would be expected.

As is clear from Figure 6, the advantage of this model is additional control over the deposition behavior before the steady state is reached. When one alters the rates in the mean field method, one necessarily changes the final coverage. However, with time-varying deposition rates, the final coverage can be kept constant while changing the time-scale of the convergence, and also the shape of that convergence (how high the rate of change in the coverage is, and at which point in the deposition prior to the steady state being reached). The control over the relationship between $\rho(t)$ and its first derivative is what creates this meaningful difference, even when the time-axis is arbitrary.

Altering the scaling factor s, we can exercise similar control over the deposition behavior, as seen in Figure 7. The change is in the initial deposition rate, while α_1 is kept constant at a moderate rate of convergence, $\alpha_1 = 10$. The most important feature to note is that time-varying rates allow for difference from the mean field result in both directions. Given a negative scaling factor s, as with the green line in Figure 7, the convergence to the steady state can be made slower than the mean field solution. Note that the same overshooting behavior seen in Figure 6 for slow exponential decay appears

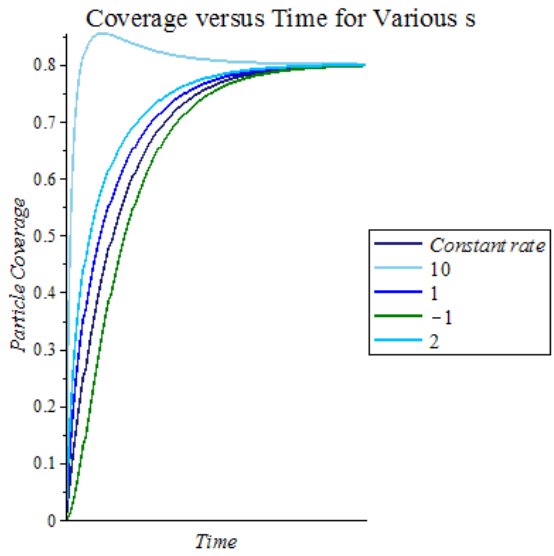

Figure 7. Particle density as a function of time for various s and the mean field solution; $\gamma = 0.5$, $\beta = 1$, $z = 4$, $\alpha_1 = 10$, $\alpha_f = 2$

here for a high scaling constant (a large difference between initial and final deposition rates). The two and be altered together for even more subtle control of the deposition.

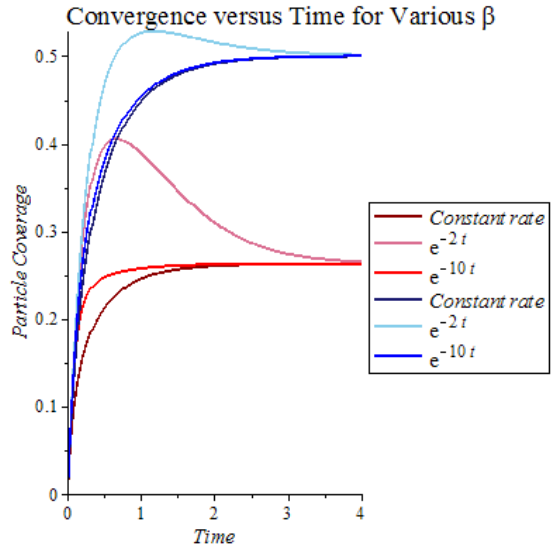

Figure 8. Particle density as a function of time for various $\beta(t)$ and the mean field solution; $\gamma = 0.5$, $z = 4$, $s = 2$, $\alpha = 2$

For illustrative purposes, I include Figure 8 in which $\beta(t)$ is varied while α is held constant. $\beta(t) = (s_\beta e^{\beta_1 t} + 1)\beta_f$, and so this plot is analogous to Figure 6, but with only the cooperative effect in the deposition changing. There are two seperate sets of data, with the darkest lines representing the constant cooperative effect mean field result. In all runs, $\beta(0) = 1$. For the red plots, $\beta(t) = (e^{\beta_1 t} + 1)0.5$, which in the blue plots

$\beta = (9e^{\beta_1 t} + 1)\beta_f$. The two sets differ in both s_β (the scaling factor) and β_f so as to keep $\beta(0) = 1$ for both sets. Note again that the same overshooting seen in Figure 6 and Figure 7 can be achieved by manipulating $\beta(t)$. Here, this is the result of a lack of initial cooperative effect, and so the deposition is not screened as strongly as it is for later time steps, when it begins to find its equilibrium with the evaporation rate. This represents another potentially useful way to alter the convergence behavior of the system.

It should also be noted again that including a decaying exponential as the time-varying portion of the deposition rate is just one way of treating this that seems particularly intuitive and potentially useful. The shape and time-scale of the convergence can be altered with even greater variety through the use of other sorts of functions. Some alternative may prove to be more valuable for modeling ISAM, and certainly other potential applications could intuitively lead to a different selection.

7. Conclusions

The survey of CSA / CSAE models included here demonstrates the clear advantage of the mean field approach, though at the sacrifice of an analytically soluble solution, and with a decoupling assumption. Additional data is required before a clear deposition trend can be determined in ISAM, but it is clear that the first several seconds result in the steady state being reached. Since this region is not currently well investigated, the convergence behavior to the steady state of the system cannot be clearly seen. This being the case, the mean field method without time-dependent rates is adequate to the task of experimental description at present.

While the time-scale is arbitrary for these models, and so the mean field method could be made to converge arbitrarily quickly, the shape of this convergence cannot be changed without time-dependent rates. A more complete experimental picture could call for qualitatively different convergences. Other applications could also benefit from this versatility.

The features of the model used here, with a decaying exponential, are very intuitive and have several desirable traits. The convergence to the steady state can be easily tuned, and one can even include an initial overshooting of the steady state. The convergence shape can then be dealt with independent of the steady state, which cannot be done using only constant rates.

One important area of further study is the experimental time-dependence of ISAM. Further, if the effective charge of individual silica nanoparticles were determined, then a more rigorous attempt at supplying cooperative effects would be possible. Further alterations to the mean field method could be useful for some systems, and the application of the method to systems with intuitive time-varying "deposition" rates would be even more appropriate than the use here with ISAM. Attempts to apply this model to such situations would be particularly valuable moving forward.

Appendix A.

For the Ising model, the equilibrium properties can be directly derived from the partition function, Z. The properties of the model prior to equilibrium depend on the spin dynamics of the system. Recall that we related the flip-rates to our node occupancy model as follows:

$$c = \gamma(\frac{1+s_i}{2}) + (\frac{1-s_i}{2})\alpha\beta^{\sum_{j\in NN}\frac{1+s_j}{2}} \tag{A.1}$$

We are free to choose the flip rates (and therefore the evaporation and deposition rates) at our discretion, but we are limited by the detailed balance condition, which states:

$$P_{eq}(s)c_i(s) = P_{eq}(s^i)c_i(s^i) \tag{A.2}$$

where s denotes some configuration of the system as a hole, and s^i denotes the same configuration with the ith spin flipped. P_{eq} is the Boltzmann factor:

$$P_{eq} = \frac{e^{-H/kT}}{Z} \tag{A.3}$$

We introduce the following notations:

$$K = \frac{J}{kT} \tag{A.4}$$

$$h = \frac{B}{kT} \tag{A.5}$$

We now solve K and h from the detailed balance condition. As will be seen, h will depend on the number of connections present between nodes. The solution below is specifically for a Cayley tree of coordination number z. The detailed balance condition becomes:

$$\frac{c_i(s)}{c_i(s^i)} = \frac{\gamma(\frac{1+s_i}{2}) + (\frac{1-s_i}{2})\alpha\beta^{\sum_{j\in NN}\frac{1+s_j}{2}}}{\gamma(\frac{1-s_i}{2}) + (\frac{1+s_i}{2})\alpha\beta^{\sum_{j\in NN}\frac{1+s_j}{2}}} = \frac{P_{eq}(s^i)}{P_{eq}(s)} = \frac{e^{-Ks_i\sum_{j\in NN}s_j - hs_i}}{e^{Ks_i\sum_{j\in NN}s_j + hs_i}} \tag{A.6}$$

The solution now requires that we plug in at least two different spin configurations, providng a system of equations with two unknowns: K and h. Consider a node on a Cayley tree of arbitrary coordination number z. There is a state for which all spins are spin-up on this tree, and a state for which all spins but one are spin-up on this tree (with this exception being a spin other than the central spin).

$$\text{All spin-up} : \frac{c_i(s)}{c_i(s^i)} = \frac{\gamma}{\alpha\beta^z} = e^{-2zK-2h} \tag{A.7}$$

$$\text{All but one spin-up} : \frac{c_i(s)}{c_i(s^i)} = \frac{\gamma}{\alpha\beta^{z-1}} = e^{-2(z-2)K-2h} \tag{A.8}$$

After some algebra, we have:

$$\text{All spin-up} : -2zK - 2h = ln(\frac{\alpha\beta^z}{\gamma}) \tag{A.9}$$

$$\text{All but one spin-up} : -2(z-2)K - 2h = ln(\frac{\alpha\beta^{z-1}}{\gamma}) \tag{A.10}$$

And so by subtracting the latter equation from the former and applying a few rules pertaining to logarithms, we extract:

$$K = \frac{1}{4}ln(\beta) \tag{A.11}$$

By substituting this value for K into either equation, we can then isolate the expression for h:

$$h = \frac{1}{4}ln(\frac{\alpha^2\beta^z}{\gamma^2}) \tag{A.12}$$

Acknowledgements

Special thanks to Brian Simpson and Mohammad Abudayyeh for their ISAM preparation and SEM work towards the preliminary experimental time-dependence results, and to Eric Schwen for his Maple template for solving and plotting differential equations.

This work would not have been possible without the help of my thesis / research / academic advisor Professor Irina Mazilu. Not only was she vital in developing, refining, and editing this work, but she has been a source of support and guidance throughout my entire undergraduate career.

References

[1] Mazilu D A, Mazilu I, Seredinski A M, Kim V O, Simpson B M, and Banks W E, *J. Stat. Mech.* P09002 (2012).

[2] Di Ventra M, Evoy S, and Heflin J R, *Introduction to nanoscience and technology*, New York: Springer (2004).

[3] Yancey S E, Zhong W, Heflin J R, and Ritter A L, *J. Appl. Phys.* **99**, 034313 (2006).

[4] Evans J W, *Rev. Mod. Phys.* **65**, 1281 (1993).

[5] Cadilhe A, Araujo N A M, and Privman V, *J. Phys. Cond. Mat.* **19** (2007).

[6] Cadilhe A and Privman V, *Mod. Phys. Lett. B* **18**, 207 (2004).

[7] Privman V, *Nonequilibrium statistical mechanics in one dimension*, Cambridge University Press, Cambridge, England (1997).

[8] Matin L F, Aghamohammadi A, and Khorrami M, *Eur. Phys. J. B* **56**, 243 (2007).

[9] Alimohammadi A and Olanj N, *Physica A*, **389**, 549 (2010).

[10] Gouet R and Sudbury A, *J. Stat. Phys.* **130**, 935 (2008).

[11] Hecht S and Frechet J M J, *Angew. Chem. Int. Ed.* **40**, 74 (2001).

[12] Kohle P, Misra E, Kannana R M, Kannanb S, and Lieh-Lai M, *I. J. Pharm.* **259**, 143 (2003).

[13] Yancey S E, Zhong W, Heflin J R, and Ritter A L, *J. Appl. Phys.* **99**, 034313 (2006).

[14] Murray J D, *Mathematical Biology I: An Introduction*, Berlin: Springer-Verlag (2002).

[15] Piqueira J R C and Araujo V O, *Appl. Math. Comput.* **213** 355, (2009).

[16] Tome T and Oliveira M J, *J. Phys. A: Math. Theor.* **44**, 095005 (2011).
[17] Mazilu D A, Mazilu I, Banks W E, Schwen E, Seredinski A M, (paper in progress).
[18] Cook L J, Mazilu D A, Mazilu I, Simpson B M, Schwen E, Kim V, Seredinski A M, *Phys. Rev. E*, (submitted, March 2014).
[19] Reif F, *Fundamentals of Statistical and Thermal Physics*, Long Grove, IL: McGraw Hill (1965).
[20] Mélin R, Anglès d'Auriac J C, Chandra P, and Douçot B, *J. Phys. A: Math. Gen.* **29**, 5773 (1996).